Molecular Cell

Article

Extended and dynamic linker histone-DNA Interactions control chromatosome compaction

Graphical abstract

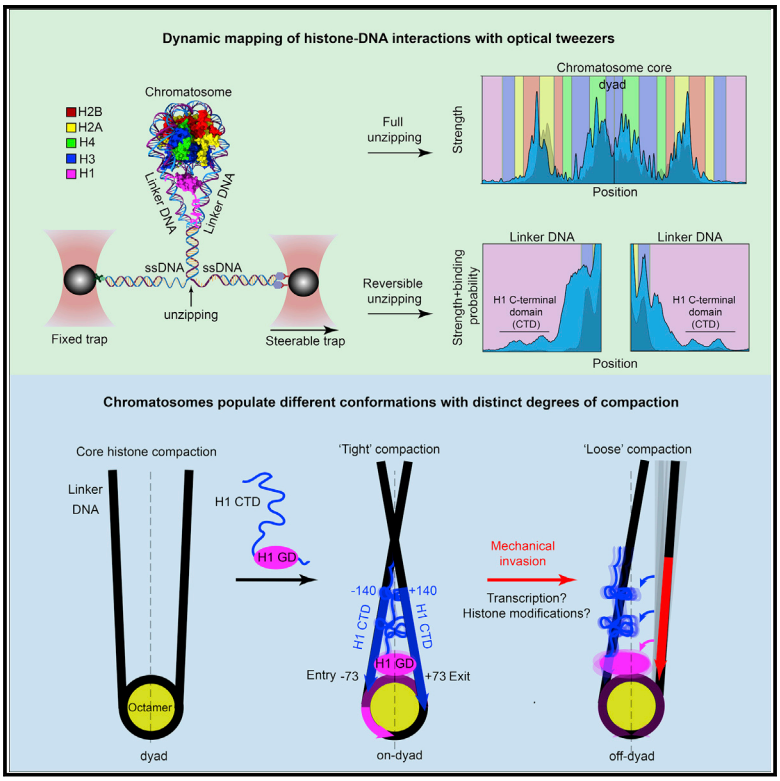

Highlights

- Single-molecule optical tweezers map histone-DNA interactions in a chromatosome
- The C-terminal domain of H1 binds both linker DNAs dynamically and extensively
- Three-contact and two-contact binding modes can exist in the same chromatosome
- Interactions at the linker DNA modulate the transition between the binding modes

Authors

Sergei Rudnizky, Hadeel Khamis, Yuval Ginosar, Efrat Goren, Philippa Melamed, Ariel Kaplan

Correspondence

akaplanz@technion.ac.il

In brief

Using single-molecule optical tweezers, Rudnizky et al. map the structure and dynamics of histone-DNA interactions in a chromatosome at nearly base-pair resolution. A single chromatosome can populate different conformations with distinct degrees of compaction, and transitions between them are modulated by H1-DNA contacts, supporting a dynamic regulatory role for H1.

Rudnizky et al., 2021, Molecular Cell *81*, 3410–3421
August 19, 2021
https://doi.org/10.1016/j.molcel.2021.06.006

CellPress

CellPress

Molecular Cell

Article

Extended and dynamic linker histone-DNA Interactions control chromatosome compaction

Sergei Rudnizky,[1] Hadeel Khamis,[1,2] Yuval Ginosar,[1] Efrat Goren,[1] Philippa Melamed,[1,3] and Ariel Kaplan[1,3,4,*]
[1]Faculty of Biology, Technion–Israel Institute of Technology, Haifa 32000, Israel
[2]Faculty of Physics, Technion–Israel Institute of Technology, Haifa 32000, Israel
[3]Russell Berrie Nanotechnology Institute, Technion–Israel Institute of Technology, Haifa 32000, Israel
[4]Lead contact
*Correspondence: akaplanz@technion.ac.il
https://doi.org/10.1016/j.molcel.2021.06.006

SUMMARY

Chromatosomes play a fundamental role in chromatin regulation, but a detailed understanding of their structure is lacking, partially due to their complex dynamics. Using single-molecule DNA unzipping with optical tweezers, we reveal that linker histone interactions with DNA are remarkably extended, with the C-terminal domain binding both DNA linkers as far as approximately ±140 bp from the dyad. In addition to a symmetrical compaction of the nucleosome core governed by globular domain contacts at the dyad, the C-terminal domain compacts the nucleosome's entry and exit. These interactions are dynamic, exhibit rapid binding and dissociation, are sensitive to phosphorylation of a specific residue, and are crucial to determining the symmetry of the chromatosome's core. Extensive unzipping of the linker DNA, which mimics its invasion by motor proteins, shifts H1 into an asymmetric, off-dyad configuration and triggers nucleosome decompaction, highlighting the plasticity of the chromatosome structure and its potential regulatory role.

INTRODUCTION

In eukaryotes, genomic DNA is packaged into nucleosomes, comprising ~147 base pairs (bp) of DNA wrapped ~1.65 times around an octamer of the core histone proteins H3, H4, H2A, and H2B (Kornberg, 1974; Kornberg and Thomas, 1974; Luger et al., 1997) and arranged as "beads on a string" separated by linker DNA (Olins and Olins, 1974, 2003). Further organization is supported by one of several linker histones (H1s) (Noll and Kornberg, 1977), which bind the nucleosome to form a chromatosome (Simpson, 1978), facilitating the formation of higher-order structures (Finch and Klug, 1976; Woodcock and Dimitrov, 2001) and promoting liquid-liquid phase separation (Gibson et al., 2019). Despite the central role that linker histones play in organizing and regulating the chromatin structure, a molecular understanding of their function is only starting to emerge (Fyodorov et al., 2018; Gilbert, 2019; Öztürk et al., 2020; Prendergast and Reinberg, 2021; Torres et al., 2016; Willcockson et al., 2021; Yusufova et al., 2021).

Eleven subtypes of linker histones have been identified in humans and mice, and they share a conserved structure, composed of a winged-helix globular domain (GD) flanked by unstructured and intrinsically disordered short N-terminal (NTD) and long C-terminal domains (CTD) (Allan et al., 1980; Fyodorov et al., 2018). The exact position and nature of the interactions between H1 and the nucleosome remain controversial (An et al., 1998; Hayes et al., 1994; Öztürk et al., 2018a; Pruss et al., 1996; Syed et al., 2010; Widom, 1998), and their precise contribution to chromatin compaction is a matter of debate (Caterino et al., 2011; Perišić et al., 2019; White et al., 2016; Zhou et al., 2015). Available structures show two binding modes for the GD, which differ in their symmetry relative to the dyad (the center of the nucleosomal DNA). In the "on-dyad" mode, the GD binds the nucleosome at three distinct DNA binding sites: one at the center and the other two at the entry and exit positions (Bednar et al., 2017; Garcia-Saez et al., 2018; Zhou et al., 2015, 2021). In the "off-dyad" mode, the GD interacts with the nucleosome at two primary locations: ~10 bp off-dyad and with a single DNA linker (Song et al., 2014; Zhou et al., 2013). A previous study showed that the orientation of H1 is dictated by the amino acid sequence specific for a subtype (Zhou et al., 2016); however, both binding modes were observed for the same variant using different experimental approaches (An et al., 1998; Hayes et al., 1994; Öztürk et al., 2018a; Pruss et al., 1996; Syed et al., 2010; Widom, 1998). Even more intriguing is the nature and extent of the CTD interactions with the nucleosomal DNA. Earlier studies indicated that although the CTD is intrinsically disordered, it becomes partially ordered when engaged with the DNA (Caterino and Hayes, 2011; Clark et al., 1988; Roque et al., 2009). In contrast, more recent studies show that the CTD remains disordered (Gibbs and Kriwacki, 2018; Heidarsson et al., 2020; Turner et al., 2018). Moreover, while a cryo-electron microscopy (EM) study showed that the CTD is associated with only a single linker DNA (Bednar et al., 2017), previous hydroxyl-radical footprinting (Syed et al., 2010) and recent nuclear magnetic resonance (NMR) experiments revealed interactions with both (Zhou et al., 2021).

The exterior positioning of H1 on the nucleosome makes it highly mobile (Brown et al., 2006; Catez et al., 2006), promoting structural plasticity of chromatin fibers (Bednar et al., 2017; Garcia-Saez et al., 2018; Song et al., 2014). At the level of a single nucleosome, H1 suppresses the spontaneous wrapping and unwrapping ("breathing fluctuations") of linker DNA (Bednar et al., 2017) and accelerates the folding of the outer wrap (Li et al., 2016). However, H1 can also spontaneously detach from the linker DNA (Bednar et al., 2017; Bernier et al., 2015), leading to increased breathing of the entire particle. These transitions were recently shown to play a critical role in transcription regulation (Bernier et al., 2015; Li et al., 2016); however, their dynamic nature presents a challenge for studying the chromatosome structure using traditional biochemical approaches, with their inherent ensemble averaging. Moreover, high-resolution structural studies often require truncation of H1 and shortening of the linker DNA, or even cross-linking, thus obscuring the underlying and functionally important dynamics.

In a previous work, Wang and colleagues used a single-molecule approach based on DNA unzipping with optical tweezers to map the strength of histone-DNA interactions inside the nucleosome (Hall et al., 2009). This approach was later used to study the properties of centromeric nucleosomes (Dechassa et al., 2011) and nucleosomes containing the variant H2A.Z (Rudnizky et al., 2016) and how the structure of the nucleosome affects the crossing dynamics of polymerase II (Pol II) (Chen et al., 2019). We further exploited this idea and developed an assay to measure the dynamic repositioning of a nucleosome by "partial" DNA unzipping (Rudnizky et al., 2016, 2019). Unfortunately, the application of these approaches to chromatosomes is challenged by the spontaneous dissociation of linker histones under single-molecule conditions (Claudet et al., 2005). In our current work, we bypassed this problem by reconstituting chromatosomes *in situ*, under single-molecule conditions, using a laminar flow cell (Malik et al., 2017; Rudnizky et al., 2018). Subjecting chromatosomes to DNA unzipping revealed that the stabilization and symmetry of their structure are supported by extended and dynamic interactions. Although a symmetric and compact on-dyad structure is the more stable one, other configurations form upon perturbation of these interactions, such as phosphorylation of specific residues or invasion by cellular machinery. Together, these results shed light on the contribution of different structural elements to the dynamic control of DNA packaging and highlight a potential regulatory role for the chromatosome.

RESULTS

DNA unzipping reveals nucleosome compaction by linker histone

To study the effect of linker histone on nucleosome compaction, we reconstituted nucleosomes on the Widom 601 positioning sequence (Lowary and Widom, 1998) and ligated them to terminally modified DNA handles connected to two beads trapped by high-resolution optical tweezers (Malik et al., 2017; Rudnizky et al., 2016). After tethering a single nucleosome between the trapped beads, we exploited a laminar flow cell to move the construct to a region containing 5 nM of full-length H1° (from now on referred to as H1) to form a chromatosome *in situ*. Subsequently, we moved the chromatosomes to an H1-free channel to avoid multiple binding events or formation of non-native aggregates and immediately subjected them to full and irreversible unzipping to prevent spontaneous dissociation of H1 (Figure 1A). Propagation of the unzipping fork led to the sequential disruption of protein-DNA interactions—revealing their position and strength—starting with those associated with the linker DNA, which are not in direct contact with core histones (Figure 1B). Next, the interaction of the N-terminal part of H3 (H3-NTD), located approximately −80/−70 bp away from the dyad (at the nucleosome's entry) is disrupted. Since this interaction is highly dynamic, it is generally undetected when unzipping the nucleosome. Remarkably, following exposure to H1, the interaction was clearly detected, and the force required to disrupt this interaction was increased (Figure 1C), indicating stabilization of this contact consistent with the reported reduction of DNA "breathing" (Bednar et al., 2017). Unzipping the DNA further led to the rupture of the strong interactions between the DNA and the proximal H2A/H2B dimer located approximately −60/−40 bp off-dyad and the strongest interactions with the $(H3/H4)_2$ tetramer positioned −20 next to the dyad (Hall et al., 2009), indicating that the presence of linker histone does not alter the position of primary histone-DNA contacts. However, the force required to overcome these interactions was elevated, suggesting that H1 compacts the DNA also at the nucleosomes' core (Figures 1C and 1D). To explore this stabilization effect in a biologically relevant DNA sequence, we assembled nucleosomes using a DNA fragment of the *Cga* gene, previously shown to harbor a nucleosome *in vivo* (Rudnizky et al., 2016). When exposed to H1, we observed a similar stabilization as that observed with 601 nucleosomes (Figure 1E), both at the entry and the core, suggesting that H1 compacts similarly the nucleosomes formed on naturally occurring DNA.

Interestingly, we noticed that our ability to detect the relatively weak interactions at the linker DNA was significantly improved for *Cga* relative to 601 nucleosomes. When we analyzed the traces, it was evident that the "background" unzipping force of naked DNA was significantly reduced for *Cga* (Figure S1A), likely due to its lower GC content. Hence, in order to combine the precise nucleosome positioning provided by the 601 sequence with a reduced background that allows detection of weaker interactions at the linker DNA, we designed a new DNA construct (which we termed 601-AT) composed of the central 73 bp of 601 DNA, responsible for its positioning properties (Chua et al., 2012) and flanked by two identical ~184-bp fragments of AT-rich DNA (Figure S1B, inset). A thermodynamic model of the unzipping reaction, based on the base-pairing energy and the DNA flexibility (Bockelmann et al., 1998), predicts a substantial drop in the unzipping force within the altered regions (Figure S1B). Indeed, when we unzipped the modified DNA construct, we observed a ~6-piconewton (pN) decrease in the rupture force at the corresponding DNA regions (Figures S1A and S1C). Next, we performed several control experiments to ensure that our modulation did not affect the nucleosome's position and structure. 601-AT nucleosomes showed a single population in a gel-shift assay (Figure S1D) and positional dispersion comparable to 601 nucleosomes under single-molecule conditions (Figure S1E). Moreover, their unzipping signature showed the two known regions of strong interaction at the expected locations (Chen et al., 2019; Hall et al., 2009; Rudnizky et al., 2019), reflecting the particles' structural integrity

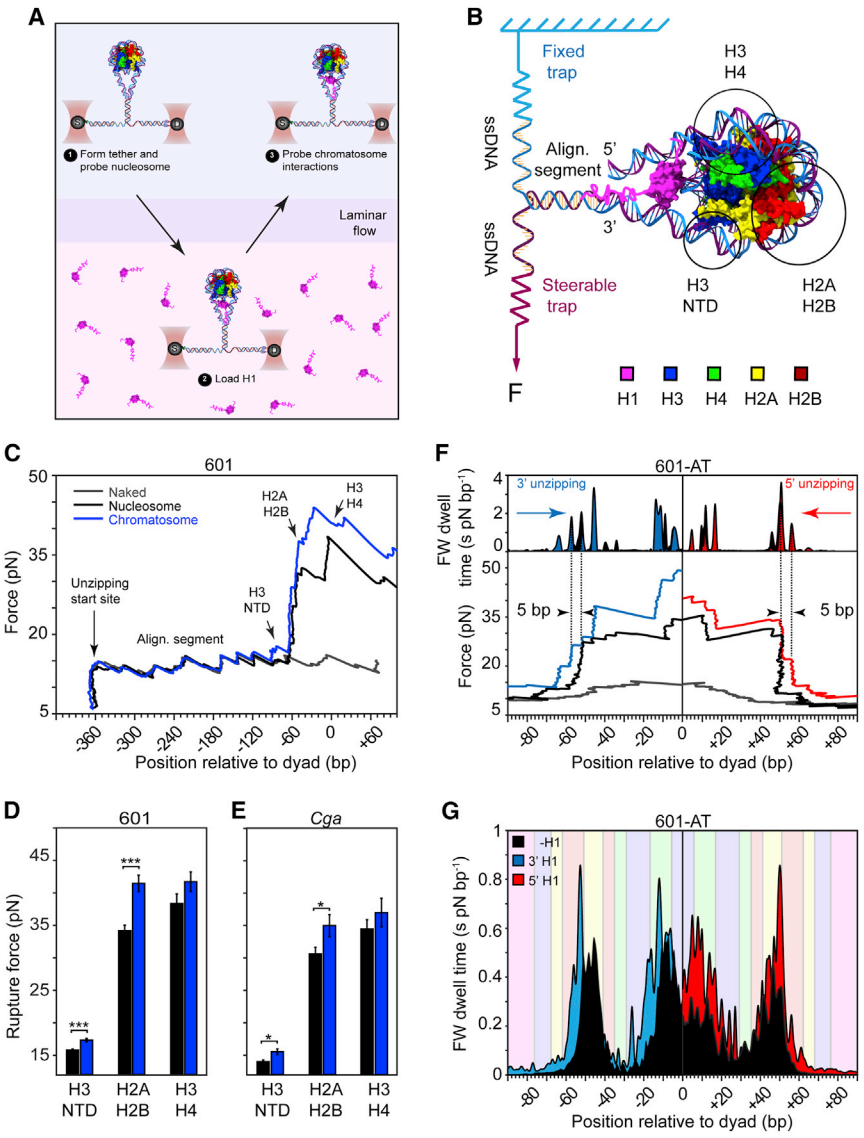

Figure 1. DNA unzipping reveals nucleosome compaction by linker histone

(A) Schematic description of the experimental assay. The nucleosome is tethered between streptavidin- (S) and anti-digoxigenin- (D) coated beads captured by dual-trap optical tweezers. The trapped nucleosome is exposed to 5 nM H1 to form a chromatosome and then subjected to DNA unzipping in the H1-free channel.

(B) Representation of the DNA unzipping reaction through a chromatosome based on the crystal structure of the GD bound to a 197-bp palindromic 601L nucleosome (PDB: 5NL0) (Bednar et al., 2017). Hypothetical positions for H1 CTDs and NTDs are shown for clarity. Two strands of the DNA are connected to DNA handles bound to the trapped S and D beads. Moving one trapped bead away from the other creates tension, leading to the conversion of double-stranded DNA (dsDNA) to single-stranded DNA (ssDNA), which allows probing the position and strength of major histone-DNA interactions (circled).

(C) Representative unzipping curves for nucleosomes reconstituted using the 601 DNA without (black) or in the presence of H1 (blue). "Naked" (i.e., no nucleosome or H1) 601 DNA (gray) is shown for reference. The unzipping reaction starts at approximately −360 bp from the dyad and proceeds through the fixed "alignment segment," reaching histone-DNA interactions in a chromatosome as highlighted in (B).

(D and E) Mean rupture forces for H3-NTD, H2A/H2B, and H3/H4 interactions, shown for 601 (D) and *Cga* (E) nucleosomes. Data shown as mean ± SEM; $n_{601} = 13$, $n_{601+H1} = 15$, $n_{Cga} = 14$, $n_{Cga+H1} = 12$. *$p < 0.05$, ***$p < 0.001$, two-sample Student's t test.

(F) Nucleosomes formed on the modified 601-AT construct were unzipped from the 3′ or 5′ end in the absence (black) or presence of H1 (blue or red, respectively). Naked DNA is shown for reference (gray). Single representative traces for each condition (bottom panel) with their corresponding force-weighted (FW) dwell time histograms (top panel) are shown for 3′ unzipping (left) and 5′ unzipping (right). Note an ~5-bp periodicity pattern of interaction in the nucleosome that is also conserved in the presence of H1.

(G) Average FW dwell time histograms constructed from multiple traces ($n_{5',-H1} = 46$, $n_{5',+H1} = 21$, $n_{3',-H1} = 53$, $n_{3',+H1} = 41$). Shaded colors (according to the color code in B) indicate positions of interactions of each histone as inferred from the crystal structure.

See also Figure S1.

(Figure S1C). Interestingly, the weak interaction of H3-NTD that was generally masked in 601 nucleosomes appeared to be more pronounced, consistent with the increased sensitivity of the 601-AT construct (Figure S1C). Finally, nucleosomes formed on 601-AT DNA were able to produce chromatosomes both in bulk and in single-molecule conditions *in situ* when we prepared them using commercially available human H1 or its bacterially expressed mouse paralog (Method details, "Chromatosome reconstitution verification"; Figures S1F–S1I).

When chromatosomes were formed *in situ* using the 601-AT construct, we observed a stabilization similar to that observed for the 601 nucleosomes but with higher sensitivity, as reflected by a ~5-bp periodicity of interactions, which were clearly stabilized in the presence of H1 (Figure 1F, bottom left panel). Conversion of the individual traces' force-position data to force-weighted (FW) dwell times (Chen et al., 2019; Hall et al., 2009) (Figure 1F, top left panel) and averaging over all the traces in the dataset (Figure 1G, left panel) allowed us to generate "compaction maps" of nucleosomal interactions stabilized by H1. They revealed that although the 5-bp periodic pattern within the interaction cluster was similar to that of nucleosomes, the magnitude of dwell times was significantly higher for chromatosomes, particularly −50 bp and −20 bp away from the dyad. Notably, these experiments probe one side of the nucleosome, which appears to be stabilized by H1, and therefore cannot rule out that H1 binds the nucleosome asymmetrically in the

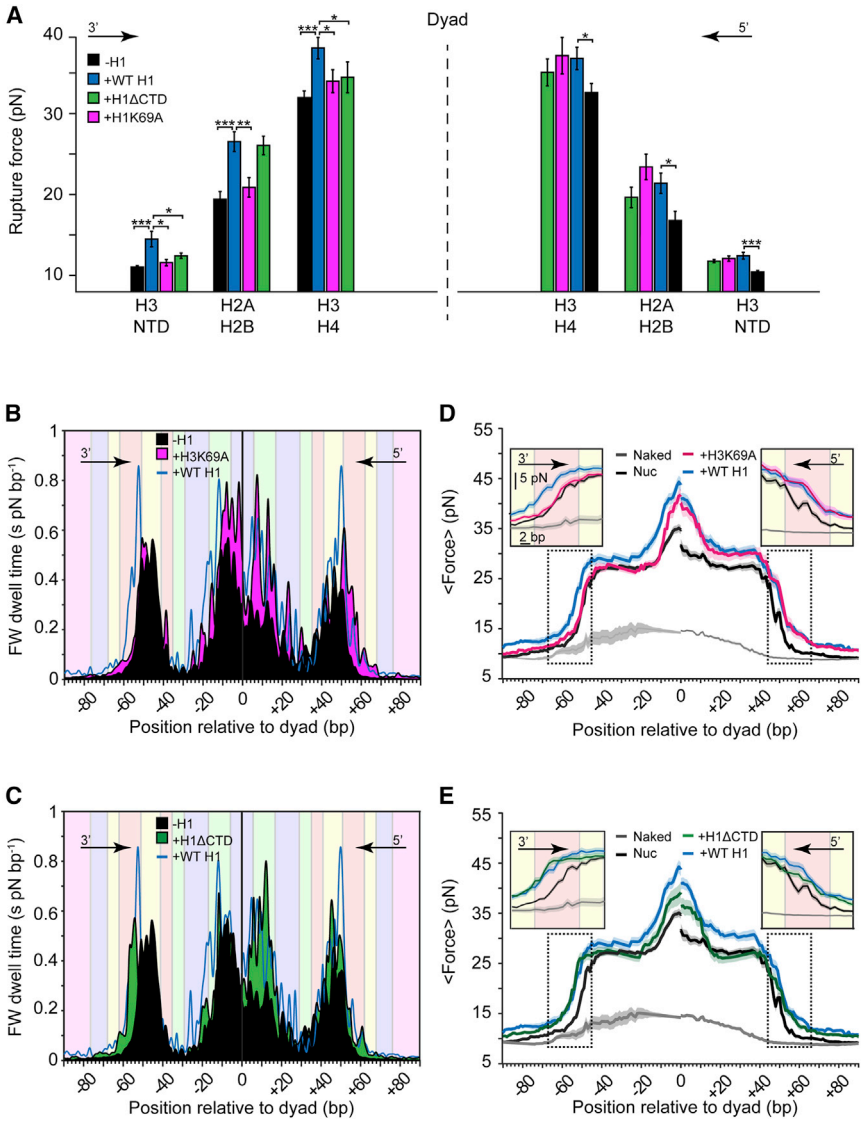

Figure 2. H1-DNA contacts at the dyad are responsible for symmetric compaction

Unzipping traces obtained from 3′ and 5′ unzipping experiments with the H1K69A (magenta) and H1ΔCTD (green) mutants were analyzed and are presented as (A) mean rupture force of regions of interactions, (B and C) FW dwell time histograms, and (D and E) average force-position curves. FW dwell time histograms of nucleosomes (black) and chromatosomes formed with WT H1 (blue) are identical to those in Figure 1G and are shown for reference. $n_{5'\text{-H1}} = 46$, $n_{5'\text{nuc+H1}} = 21$, $n_{3'\text{-H1}} = 53$, $n_{3'\text{nuc+H1}} = 41$, $n_{5'\text{nuc+H1K69A}} = 22$, $n_{3'\text{ nuc+H1K69A}} = 27$, $n_{5'\text{nuc+H1}\Delta\text{CTD}} = 22$, $n_{3'\text{nuc+ H1}\Delta\text{CTD}} = 20$. *p < 0.05, **p < 0.01, ***p < 0.001, two-sample Student's t test.

See also Figure S1.

"off-dyad" conformation, as proposed by several previous studies (An et al., 1998; Pruss et al., 1996; Song et al., 2014; White et al., 2016; Zhou et al., 2013). However, when we unzipped the complexes from the opposite (5′) end, we observed a similar stabilization of the H3-NTD contact as with the 3′ end unzipping experiments (Figures 1F and 1G, right panel, and 2A), indicating that H1 contacts the DNA on both sides of the nucleosome. Moreover, the H3/H4 and H2A/H2B regions were stabilized to a similar extent in the 3′ side, suggesting that H1 binds the nucleosome in an on-dyad configuration, compacting the entire structure symmetrically.

H1-DNA contacts at the dyad modulate the symmetry of compaction

To understand what region in H1 is responsible for the symmetric compaction, we decided to focus on the dyad-binding residues. Among them is a conserved lysine at position 69, which interacts with 1 of the 7 bp at the nucleosome center (Bednar et al., 2017) and is crucial for H1 binding *in vitro* (Zhou et al., 2015) and *in vivo* (Brown et al., 2006). To test whether this contact is involved in the observed stabilization, we mutated it to alanine and expressed the altered H1 (H1K69A) in *E. coli* (Figure S1F). We then used the purified variant to form chromatosomes *in situ*, followed by DNA unzipping from the 5′ or 3′ orientation. When probed in the 5′ direction, binding of the mutated H1 resulted in a similar stabilization of the nucleosome as with wild-type (WT) H1, as indicated by higher forces and elevated dwell times within the H2A/H2B and H3/H4 regions (Figures 2A and 2B, right panels). However, when we examined chromatosomes from the 3′ end, the stabilization of the dyad interaction was significantly reduced (Figures 2A and 2B, left panels) not only for the H3/H4 region proximal to the mutated lysine 69, but also for the relatively distant H2A/H2B contacts. This asymmetry between 3′ and 5′ halves was clearly seen also in average force-position curves (Figure 2D). Strikingly, even the more distant H3-NTD-DNA interaction, located ~80 bp away from the mutated position, was reduced in the 3′ side (Figures 2A, 2B, and 2D). Together, this indicates that an alternative, asymmetric stable conformation exists and suggests that the residues at the dyad are essential for stabilizing the symmetric "on-dyad" configuration. This result is consistent with a previous study that showed that residues close to the dyad could determine whether the chromatosome is in the on- or off-dyad mode (Zhou et al., 2016).

Conversely, previous studies showed that truncation of the CTD does not affect the binding orientation (Bednar et al., 2017; Zhou et al., 2015, 2016). Hence, to further explore the contribution of the H1 CTD to the observed stabilization, we expressed and purified the 1–97 amino acid fragment of H1 lacking

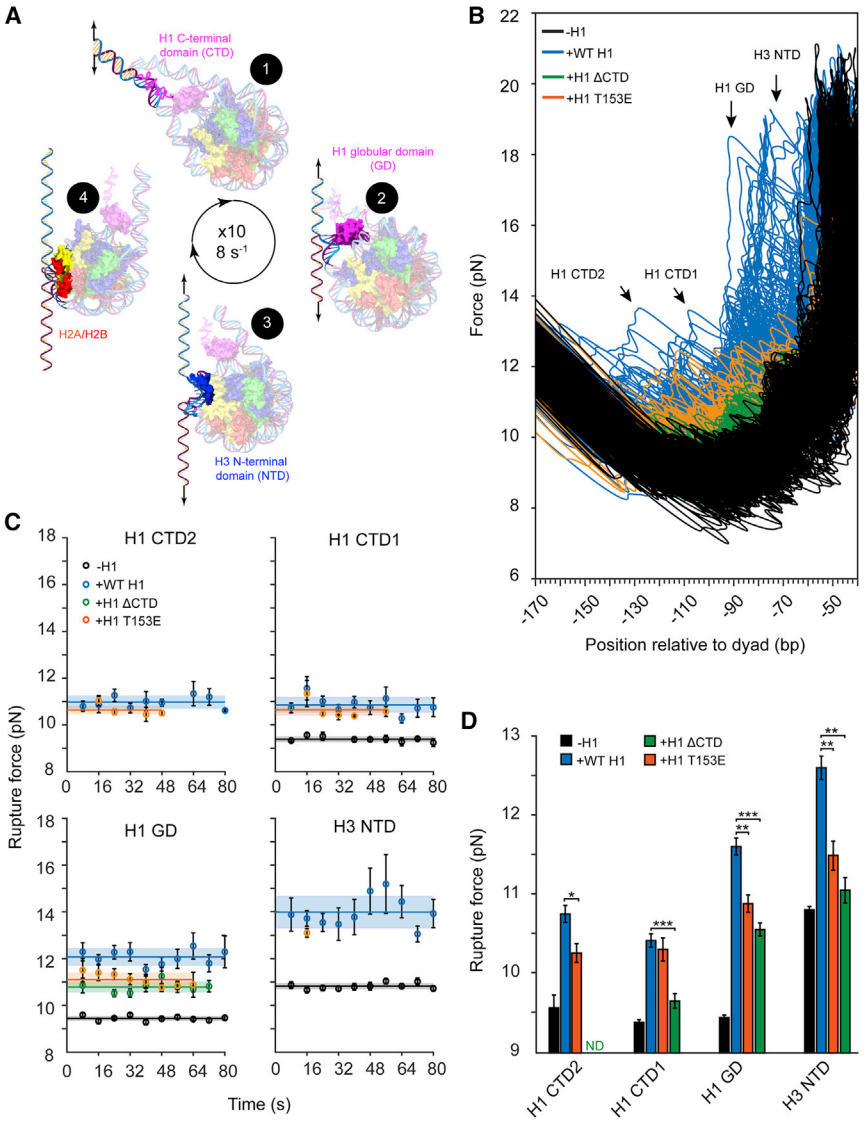

Figure 3. Dynamic mapping uncovers extended interactions of the H1 CTD and their role in nucleosome compaction

(A) Schematic description of the reversible unzipping assay to probe H1 interactions with linker DNA. Progression of the unzipping fork displaces H1 directionally, starting with (1) the CTD, followed by (2) the GD and (3) H3-NTD, until reaching (4) an H2A/H2B dimer. Next, the tension is relaxed, and dsDNA is reformed, after which the unzipping cycle is repeated (10 times, 8 s per cycle).

(B) Repetitive unzipping force-extension curves of the WT (blue), H1ΔCTD (green), and H1T153E (orange) chromatosomes or nucleosomes without H1 (black), all unzipped from the 3′ direction. The WT chromatosomes were probed under STO conditions. The H1ΔCTD and H1T153E binding to nucleosomes was unstable over time (Figure S2C) and hence investigated using MTO conditions. The clusters of detected interactions are highlighted with arrows.

(C and D) The interactions measured in each unzipping cycle (see Method details) were quantified and presented as (C) mean rupture forces as a function of time within an 8-s window and (D) mean rupture forces. Only data calculated from more than two data points (i.e., two bound events) are shown. Data are shown as mean ± SEM; n_{nuc} = 318, $n_{nuc+WT\ H1}$ = 250, $n_{nuc+H1\Delta CTD}$ = 41, $n_{nuc+H1T153E}$ = 54. *$p < 0.05$, **$p < 0.01$,***$p < 0.001$, two-sample Student's t test.

See also Figures S1, S2, S5, and S6.

the CTD (H1 ΔCTD; Figure S1F; Table S5) and repeated the unzipping experiments with the truncated variant. Although we observed a clear destabilization at the entry, and a subtle one at the core and exit regions, H2A/H2B contacts remained stabilized symmetrically around the dyad, similarly to when chromatosomes contained the WT H1 (Figures 2A, 2C, and 2E). This implies that although the CTD encompasses almost half of H1, it does not affect the symmetry of compaction but instead supports the existing H1-DNA contacts.

Dynamic mapping uncovers extended interactions of H1 CTD and linker DNA

The weakening of chromatosome compaction upon the deletion of the CTD motivated us to explore further the nature of the H1 CTD interaction with a nucleosome. We decided to focus on contacts with the linker DNA, where the CTD was proposed to bind (Bednar et al., 2017; Syed et al., 2010; Zhou et al., 2021). Although the presence of interactions in this region was evident from the initial experiments, their relatively weak rupture forces and likely rapid dynamics prevented us from systematically studying them using an irreversible unzipping experiment. Hence, we developed an assay based on partial unzipping that probes the position and strength of H1-linker DNA interactions multiple times in the same molecule. Of note, repetitive partial unzipping does not destabilize the nucleosome or induce repositioning, as shown in our previous work (Rudnizky et al., 2019). Nucleosomal DNA was unzipped until reaching, but not disrupting, the proximal H2A/H2B interaction (typically ~19 pN). After the interaction was detected, the force was relaxed again and the construct rezipped (Figure 3A). Next, the same nucleosome complex was exposed to H1 to form a chromatosome, moved to a region of the laminar flow cell depleted of H1, and subjected to ~10 cycles of reversible unzipping (~8 s for each cycle). Data collection efficiency using multiple unzipping cycles was now significantly increased. Furthermore, our data analysis was significantly improved by using control experiments with the same nucleosome for alignment.

Unzipping curves now clearly showed the presence of force rips in the linker DNA region, which can be clustered into four defined areas of interactions (Figure 3B). The mean rupture force

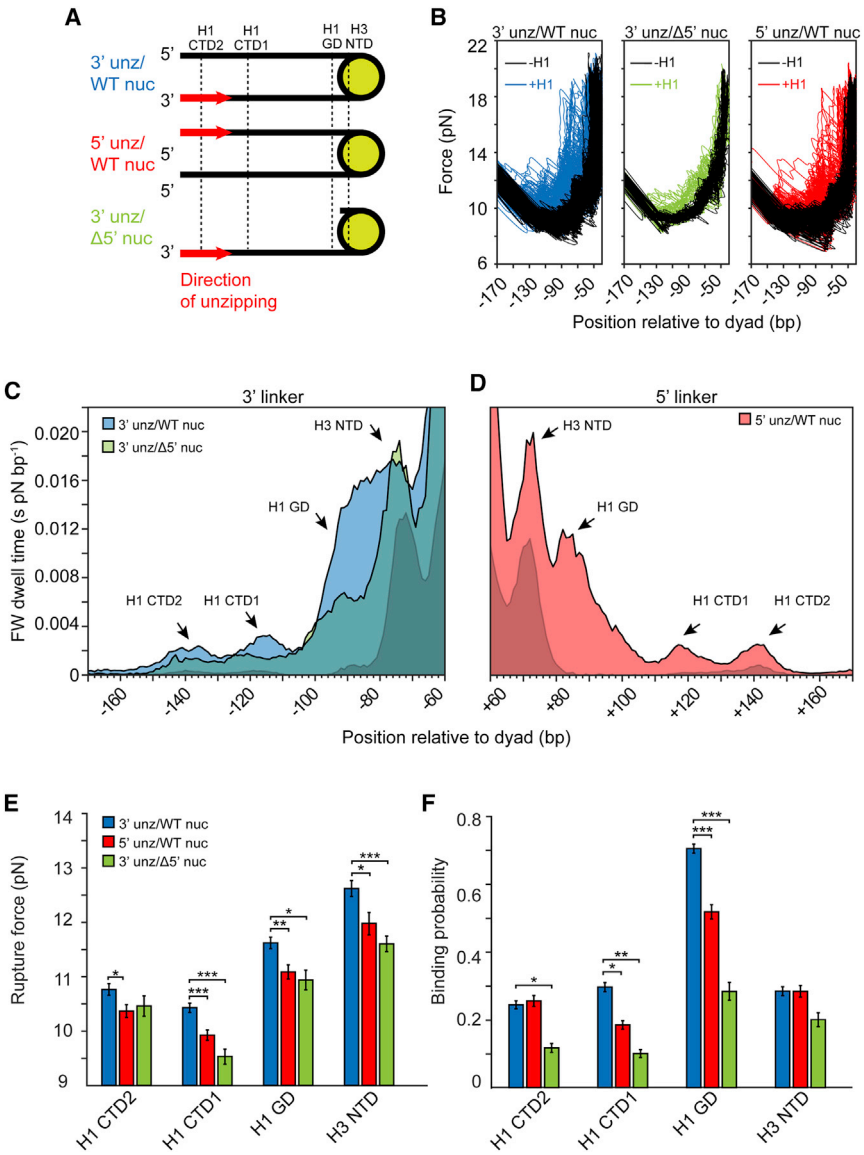

Figure 4. H1 dynamically interacts with both linkers to stabilize the on-dyad conformation

(A) Molecular constructs used for repetitive unzipping experiments. 3′ unz/WT nuc, WT nucleosome unzipped from 3′ end; 5′ unz/WT nuc, WT nucleosome unzipped from 5′ end; 3′ unz/Δ5′ nuc, nucleosome harboring a full 3′ linker to be unzipped, but with a 3-bp-long 5′ linker designed to abolish interactions with GD, CTD1, and CTD2.

(B) All traces of WT or single-linker chromatosomes unzipped partially from the 3′ or 5′ direction used for further analysis in (C) and (F). Corresponding control experiments without H1 are shown in black. Traces with chromatosomes formed with WT H1 (3′ unz/WT nuc, blue) are identical to those in Figure 3B and are shown for reference.

(C and D) Average FW dwell time histograms constructed from partially unzipped traces (~10 cycles, 8 s each) for Δ5′ chromatosomes (C) (green) and WT chromatosomes probed from the 3′ (C) (blue) and 5′ (D) (red) directions. Control experiments without H1 are shown in black as a reference. All traces were low-pass filtered to 150 Hz and binned to 1 bp. The clusters of detected interactions are highlighted with arrows.

(E and F) Rupture forces (E) and binding probabilities (F) calculated for the clustered interactions, as shown in (C) and (D). Data are shown as mean ± SEM; $n_{5'nuc}$ = 136, $n_{3'nuc}$ = 187, $n_{\Delta5'\ nuc}$ = 60, $n_{5'nuc+H1}$ = 139, $n_{3'nuc+H1}$ = 250, $n_{\Delta5'\ nuc+H1}$ = 60. *p < 0.05, **p < 0.01, ***p < 0.001; two-sample Student's t test for (E), χ^2 test for (F).

See also Figures S2, S3, and S5.

for each interaction remained constant over time (Figure 3C), suggesting that they can rapidly regain their native conformation upon relaxation and rezipping. The position of the H3-NTD contact at the entry, approximately −70 bp away from the dyad (Luger et al., 1997), was readily detected also without H1 (Figure 3B)—albeit with significantly lower forces (Figures 3C and 3D)—consistent with the quantified rupture forces measured in the previous, irreversible unzipping experiments (Figures 1D, 1E, and 2A). Three additional interaction regions upstream did not appear in the absence of H1. At approximately −90 bp, we detected an interaction region that, based on the available crystal structures (Bednar et al., 2017; Zhou et al., 2013), we attribute to the GD-linker DNA interaction. Interestingly, approximately −115 bp and −140 bp away from the dyad, we observed two previously unreported interactions, which we suspected were formed by the CTD (CTD1 and CTD2; Figures 3B and 4C). Indeed, these contacts were absent in ΔCTD chromatosomes (Figures 3B and 3D), confirming that they belong to the CTD. Gradual truncation of the CTD tail (Figures S6A and S6B) revealed that these interactions are absent in the Δ72 mutant but observed in Δ24 (Figures S6C and S6D), suggesting that they correspond to the ~120–160 amino acids in H1, where most of the S/TPXK motifs are clustered. The mean rupture force of these interactions was significantly lower than that of the GD, suggesting that the CTD is more loosely bound to the linker DNA. Similar clusters of interactions were also observed when we performed the experiments with *Cga* nucleosomes but were less pronounced than those observed for the 601 ones, likely due to the reduced sensitivity offered by this construct (Figures S2A and S2B). Notably, these newly detected contacts between H1 and linker DNA indicate that the size of the chromatosome is significantly larger than previously reported.

The CTD anchors the GD and stabilizes the nucleosome entry

Next, we aimed to explore the role of the detected CTD interactions in nucleosome compaction. However, repeating the reversible unzipping experiment with the ΔCTD mutant led to a rapid

decrease in the fraction of successive binding events (i.e., the "binding probability") over time (Figure S2C), suggesting that faster dissociation prevented us from characterizing its interactions under these single-turnover (STO) conditions. To overcome this, we incubated the nucleosome with the mutant H1 under multiple-turnover (MTO) conditions (i.e., with continuous exposure of H1) to form the complexes simultaneously. A lack of a decrease in binding probability in the GD position over time indicated the rapid formation of the complexes (Figure S2C). In contrast, the rupture forces were similar between the MTO and STO (Figure S2D), indicating that similar complexes form. Notably, in addition to eliminating the stabilization of the CTD interactions, both GD and H3-NTD interactions were significantly destabilized for the ΔCTD mutant (Figure 3D), a trend that was intensified when shortening the CTD (Figure S6D).

Having established the importance of the entire CTD, we sought to explore the contribution of individual CTD-DNA contacts. Our truncation experiments (Figure S6D), together with several reports, indicate that the CTD binds the linker DNA via specific and structured S/TPXK domains, rather than contacting it non-specifically (Caterino and Hayes, 2011; Clark et al., 1988; Roque et al., 2009). Mutation of threonine to glutamic acid, which mimics phosphorylation in this residue, reduces H1.1 binding *in vivo*, reminiscent of the effect of partial truncation of the CTD (Hendzel et al., 2004). Accordingly, we decided to substitute the conserved threonine at position 153, located at the TPKK domain in H1, with glutamic acid (H1 T153E). We expressed and purified the mutant protein, assembled the chromatosome *in situ*, and subjected it to partial unzipping analysis under MTO conditions to prevent any possible dissociation. The rupture forces associated with CTD2 and the distant GD and H3-NTD (but not CTD1) were reduced, suggesting that phosphorylation induces a global conformational change (Figures 3B–3D). Overall, these results indicate that the CTD allows H1 to stay on the DNA for a prolonged period and, once engaged, mediates the GD compaction of the nucleosome at the linker region.

H1 dynamically interacts with both linkers to stabilize the on-dyad conformation

The increase in compaction at both entry and exit sites (Figure 2A) suggests that H1 also interacts with the opposite, 5′ linker DNA. To map interactions in this region, we conducted a partial unzipping experiment from the opposite orientation (5′unz/WT nuc; Figure 4A). Contacts attributed to the GD were detected approximately +90 bp away from the dyad (Figure 4B, right panel), similar to unzipping the 3′ linker and consistent with the irreversible unzipping experiments. Interestingly, similarly to the proximal linker DNA, we detected clusters of interactions located +115 bp and +140 bp away from the dyad, suggesting that the CTD interacts with both linker arms at similar positions (Figures 4C and 4D). Quantification of the mean breaking forces of the interactions revealed slightly reduced values for both the GD and the CTD in the 5′ orientation, suggesting a weaker binding to DNA (Figure 4E).

The presence of interaction clusters at similar positions at both linkers could reflect two extreme scenarios or a combination of them. One possibility is that H1 binds both linkers similarly and concurrently, creating a "stem-like" structure, as proposed previously (Hamiche et al., 1996; Syed et al., 2010). An alternative option is that H1 dynamically switches position between the two linkers, interacting with a single linker at a time. To clarify this, we used the data from the reversible unzipping experiments to calculate the binding probability of each H1 interaction with the 5′ and 3′ linkers. All interactions showed binding probabilities lower than 1, suggesting that H1 occasionally detaches from the linker DNA. If H1 were to alternate between the proximal and distal linker DNA, we would expect the sum of the probabilities to detect any given interaction—at the 5′ and 3′ side—to be also smaller than 1. However, the binding probability of the GD contact was ~0.7 for the 3′ linker and ~0.5 for the 5′ linker (Figure 4F), suggesting that for a significant fraction of time, the GD interacts with both linkers simultaneously. To further clarify this point, we probed H1 binding to nucleosomes lacking a 5′ linker (3′unz/Δ5′ nuc; Figures 4A and S4A). In the case of simultaneous binding to two linkers, the deletion of one linker is expected to weaken the interactions with the remaining one, resulting in a *decrease* in their binding probability. In contrast, if H1 occupies only a single linker at a given time, we anticipate an *increase* in binding probability, since now the "competitor" linker is eliminated. When we partially unzipped the deletion nucleosomes in the presence of WT H1, an apparent elevation of force in the region corresponding to GD-DNA interaction was readily detected (Figures 4B, 4C, and 4E), confirming that it was able to form a chromatosome. This observation is consistent with a study showing that a nucleosome with a single linker arm is a minimal substrate for H1 binding (White et al., 2016). However, the binding probability and the breaking force of GD and CTD interactions were significantly reduced (Figures 4E and 4F), favoring the scenario in which the CTD and GD interact with both linkers simultaneously. This was not the result of H1 dissociation from the nucleosome since GD-DNA interaction was readily detected even after 80 cycles (>10 min) under the STO conditions.

Mechanical invasion into chromatosome triggers decompaction

The fact that H1 can stably bind a nucleosome harboring a single linker DNA indicates that H1 can populate an alternative conformation, distinct from the three-contact, "on-dyad" conformation of double-linker WT nucleosomes. Hence, we wondered whether WT nucleosomes were able to switch their conformation following a perturbation reducing H1-DNA interactions with one of the linkers, in a manner similar to the progression of a motor protein, such as RNA polymerase, into the chromatosome. To address this, we perturbed a chromatosome by increasing the number of partial unzipping cycles from ~10 to ~80 (Figure 5A). Single-linker chromatosomes, for which only a two-contact conformation is available, are intuitively expected to dissociate when repetitively perturbed over a long time. However, we found relatively consistent values of rupture forces (Figure 5B) and binding probability (Figure 5C) over time at all clusters of interaction, indicating that the conformation remained the same throughout the experiment. In contrast, while the mean rupture forces of all regions did not change significantly for WT nucleosomes, we observed a clear decay in binding probability as a function of time for all four regions, suggesting that H1 gradually

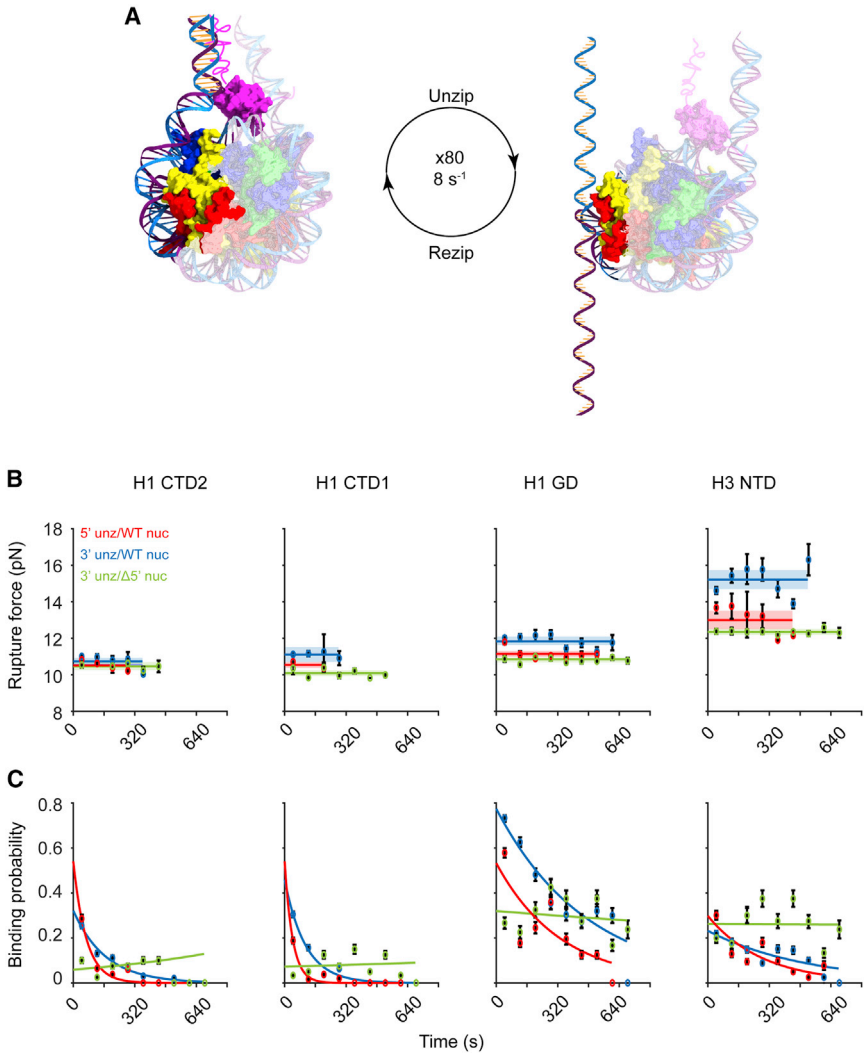

Figure 5. Mechanical invasion into a chromatosome triggers decompaction

(A) Schematic representation of the invasion experiment. The experiment was conducted similarly to the one shown in Figure 3A but with >80 unzipping cycles.

(B and C) Rupture forces (B) and binding probabilities (C) are shown as a function of time (~720 s, 80-s window) for all interaction clusters of the WT and truncated chromatosomes. Data are shown as mean ± SEM; $n_{3'\ unz/WT\ nuc}$ = 787, $n_{5'\ unz/WT\ nuc}$ = 444, $n_{3'\ unz/\Delta5'\ nuc\ CTD}$ = 354, $n_{3'\ unz/\Delta5'\ nuc}$ = 534. Exponential fits are shown to guide the eye.

See also Figure S4.

changes its conformation. Hence, prolonged perturbation of the interactions in one linker DNA can induce a global conformational change, provided that an alternative conformation exists.

Interestingly, although the decrease in binding probability for WT chromatosomes was evident in both orientations, it was more pronounced for the perturbation from the 5′ side (Figure 5C). Moreover, when we irreversibly unzipped the chromatosomes after the invasion from the 3′ and 5′ sides, the decrease in the compaction of interactions was more substantial for the 5′ side (Figure S4B). This suggests that the propagation of a motor protein into a chromatosome can displace H1 or its domains, leading to its decompaction, and it does so in an asymmetrical manner, with the chromatosome being more sensitive to invasion from the 5′ end.

DISCUSSION

In this study, we used single-molecule optical tweezers to sequentially unzip DNA harboring a chromatosome, with the aim of measuring the position and strength of H1-DNA interactions. Our experimental system overcomes several important limitations of preceding studies. First, the use of a laminar flow cell enables the single-molecule characterization of H1-nucleosome complexes in native conditions, which otherwise rapidly disassemble. Second, the directionality and reversibility of the unzipping reaction allow measurement of the position and dynamics of protein domains in the intact complex and individual perturbation of their function by prolonged unzipping. Third, measurement of the forces associated with protein-DNA interactions provides a direct assessment of the degree of compaction by H1 with high resolution and sensitivity.

Using this approach, we observed a previously unreported tightening of the H2A/H2B and H3/H4 interactions with the DNA upon H1 binding. This stabilization likely stems from the interactions of H1 at the nucleosome dyad. Two main observations support this idea. First, the K69A mutation abolishes the stabilization of H2A/H2B, located ~40 bp from the center and, hence, not directly in contact with H1. Second, probing the dyad interactions using unzipping requires prior disruption of H1 interactions with the proximal linker DNA. The increased resistance to the unzipping fork at the proximal H2A/H2B contact suggests that H1, which remains bound to the dyad, stabilizes the dimer from the inside out. This implies that H1 binding induces a conformational change in the nucleosome dyad that propagates for at least 40 bp, most probably also affecting the linker DNA. Notably, a recent structural study shows that the CTD of H2A and NTD of H3 undergo a conformational change upon the binding of H1, forcing them to interact with the DNA at the core (Zhou et al., 2021). The symmetric stabilization of both H2A/H2B dimers and entry/exit suggests that H1 binds in the on-dyad conformation. The K69A mutation leads to the disruption of this symmetry, such that only half of the nucleosome is stabilized. In addition, the interaction with one of the linkers is almost abolished, indicating that most of the H1 mass is associated with one side of the nucleosome.

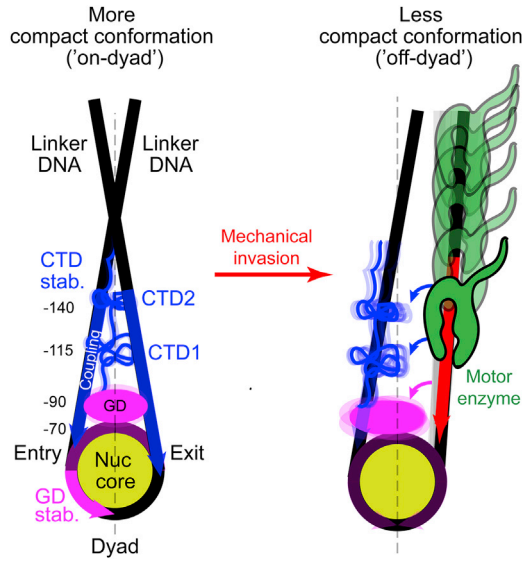

Figure 6. A model for dynamic compaction of a chromatosome particle

H1 binds the canonical nucleosome in an on-dyad conformation. Binding of the GD to the dyad induces a conformational change, leading to compaction of both H2A/H2B dimers. The CTD dynamically couples both linkers at two positions, approximately ± 110 bp and approximately ± 140 bp from the dyad, to stabilize GD-linker interactions. Mechanical invasion into the linker DNA up to the GD-DNA contact triggers H1 repositioning to the less condensed and dynamic off-dyad conformation.

The observed stabilization of the core interactions is expected to have a significant effect on the activity of polymerases, chromatin remodelers, and structural maintenance of chromosomes (SMC) complexes engaging the nucleosome. First, a difference of a few pN in the force opposing a SWI/SNF remodeler's translocation can cause a dramatic change in its remodeling efficiency (Zhang et al., 2006). Together with our data, this may explain the recently reported inhibition of imitation switch (ISWI) remodeler activity in chromatosomes (Zhou et al., 2021). In addition, Pol II overcomes the nucleosomal barrier by exploiting nucleosomal fluctuations (Hodges et al., 2009), and the transcriptional obstacle encountered by Pol II while crossing the nucleosome was shown to correlate with the barrier mapped by an unzipping assay similar to ours (Chen et al., 2019). In particular, the proximal dimer region of the nucleosome, which we show here to be stabilized by H1, is a major physical barrier for Pol II. Finally, the on-dyad orientation of a specific H1 variant, observed exclusively in metaphase (Arimura et al., 2020), was shown to inhibit condensin loading and affect chromosome compaction and individualization (Choppakatla et al., 2020), highlighting how local effects may potentially affect the global chromatin structure.

The CTD interacts with both linker DNAs, consistent with recent cryo-EM and NMR studies demonstrating that binding to both linkers occurs in several isoforms of H1 (Zhou et al., 2021). However, due to the dynamic nature of the CTD contacts, their exact positions were not mapped before. Our unzipping assay, which allows dynamic mapping of histone-DNA contacts, shows that the CTD makes focal contacts ~115 bp (CTD1) and ~140 bp (CTD2) away from the dyad, suggesting that the absolute length of the DNA that is associated with histones is ~280 bp. This is significantly longer than previously interpreted by nuclease digestion experiments (Fyodorov et al., 2018; McGhee and Felsenfeld, 1980; Simpson, 1978) and has important implications for the formation of chromatin fibers (Collepardo-Guevara and Schlick, 2014) and the promotion of phase separation by linker histones (Gibson et al., 2019). Our truncation experiments indicate that CTD1 and CTD2 reside at the center of the CTD, likely formed by the S/TPXK motifs, which can undergo a disorder-to-order transition when bound to DNA (Caterino and Hayes, 2011; Clark et al., 1988; Roque et al., 2009). Their relatively fixed position and the ability to rapidly recover following rezipping suggest that CTD1 and CTD2 are ordered rather than disordered. The distant location and dynamic nature of these interactions may explain why they have not been observed in previous studies using only shorter DNA (Bednar et al., 2017; Zhou et al., 2015).

Gradual deletion or phosphorylation of the CTD lessens the compaction of the nucleosome's entry and exit. The mechanical properties of DNA are likely to play a role in this compaction, as stabilization of a curved DNA conformation by one interaction may lower the energetic barrier for another. Indeed, we observe different degrees of compaction and symmetry as a function of the local DNA sequence (Figures S2E–S2G). Moreover, our analysis of the *conditional* binding probability for each interaction, given that one of the other interactions is present in the same probing cycle, reveals a significant degree of cooperativity between the CTD interactions and the compaction of the H3-NTD (Figure S3B). However, although this argument would predict a higher degree or cooperativity between interactions that are at shorter distances, H3-NTD is more strongly coupled with the distal CTD2 than the proximal CTD1 (Figure S3B, top panels). This suggests that the protein conformation, in addition to the DNA, is responsible for allosterically coupling CTD binding and entry/exit compaction and, thus, further supports the ordered nature of the CTD when bound to the DNA.

Our results also suggest that the cellular machinery may exploit the positional plasticity of H1 to push it to the more dynamic and less compact off-dyad mode by modulating H1 contacts with the linker DNA (Figure 6). The tendency of H1 to dissociate more rapidly from the distal side suggests that the transition of H1 can be triggered more quickly at this location. While both H1 dissociation and downstream movement can explain this observation, it is more likely that H1 remains bound to the nucleosome, consistent with previous studies (Ericsson et al., 1990; Nacheva et al., 1989). Modulation of this transition by the CTD is consistent with the distinct dynamic behavior of linker DNA observed for different isoforms of H1 (Zhou et al., 2021) and might explain their differential enrichment at particular genomic positions and distinct function (Prendergast and Reinberg, 2021).

The reduced compaction by a mimic of CTD phosphorylation, also observed in another study (Zhou et al., 2021), suggests that some of the various H1 post-translational modifications (PTMs) that occur in dyad and linker-DNA interfaces may also affect its binding orientation (Bednar et al., 2017; Christophorou et al., 2014; Öztürk et al., 2018b; Wiśniewski et al., 2007,

2008). For instance, modifications such as phosphorylation of the conserved arginine 74, which is in tight contact with linker DNA, or acetylation of lysine 73, which mapped to the dyad, can lead to electrostatic repulsion with the DNA, pushing H1 to the less energetically favorable off-dyad mode. The same is true for PTMs of the core histones that can trigger decompaction by modulating interactions with the linker DNA. For example, a recent study suggests that acetylation of H3-NTD loosens nucleosome packaging by directly affecting its interaction with the H1 CTD (Hao et al., 2020). Moreover, H3K56ac that increases nucleosome unwrapping was shown to facilitate the binding of a transcription factor to a chromatosome (Bernier et al., 2015). The fact that the binding conformation can be modified by diverse mechanisms—including PTMs, length of DNA linker, and stereochemical constraints—may explain the distinct binding modes observed for the same variant in different studies (An et al., 1998; Hayes et al., 1994; Öztürk et al., 2018a; Pruss et al., 1996; Syed et al., 2010; Widom, 1998), as also pointed out in a recent review (Prendergast and Reinberg, 2021).

Collectively, our study suggests that a single H1 subtype can adopt both the on-dyad and off-dyad orientations, with the on-dyad being more energetically favorable (Öztürk et al., 2020; Woods and Wereszczynski, 2020), and transitions between these conformations can be triggered by cellular cues affecting H1 contacts at the dyad or with the linker DNA. Chromatosome orientation can also play a role since decompaction is triggered more easily from the distal linker. As the off-dyad mode is associated with a less compact nucleosome, this offers the possibility that the chromatosome conformation functions as a global modulator of chromatin processes. From a broader perspective, dynamic changes in the H1 contact orientation likely affect the higher-order assembly of neighboring chromatosomes into chromatin fibers, as predicted by theoretical modeling (Depken and Schiessel, 2009) and simulations (Perišić et al., 2019) and shown by recent cryo-EM structures (Bednar et al., 2017; Garcia-Saez et al., 2018; Song et al., 2014). Dependence of these transitions on the modifications mentioned above may explain the absence of the canonical higher-order structures instead of which heterogeneous "clutches-like" structures are observed *in vivo* (Ou et al., 2017; Ricci et al., 2015). Moreover, the CTD of H1 was shown to promote phase separation in a linker DNA-length-dependent manner (Gibson et al., 2019). This suggests a possible role for the extended interactions we report here in controlling the effective DNA linker length and, thus, regulating phase separation. Since various biological processes rely on precise control over DNA readout, and in light of recent studies highlighting the importance of linker histones in health and disease (Willcockson et al., 2021; Yusufova et al., 2021), the ability of a cell to alter the chromatin compaction by directly modulating the chromatosome provides a means of efficient spatiotemporal control over genetic information, which is required to orchestrate a complex physiological outcome (Bar-Sadeh et al., 2020). Our work highlights how the inherent conformational plasticity of the fundamental packaging unit of chromatin may contribute to this process.

Limitations

Our study has a number of limitations. First, as with any structural study using mono-nucleosomes and mono-chromatosomes, our result may not fully capture the conformations existing in native chromatin. Second, the force required to unzip naked DNA presents a lower bound on the strength of interactions between proteins and DNA that can be detected, so weaker interactions are missing from our interaction maps. This also limits our ability to explore different linker DNA sequences, as a higher GC content correlates with a higher naked DNA unzipping force and, hence, a lower sensitivity for the detection of histone-DNA interactions. Finally, although the rupture forces measured in our study are indicative of the strength of histone-DNA interactions, they are only partially related to the magnitude of the forces applied by motor proteins, which disrupt the nucleosome structure through different reaction coordinates.

STAR★METHODS

Detailed methods are provided in the online version of this paper and include the following:

- KEY RESOURCES TABLE
- RESOURCE AVAILABILITY
  - Lead contact
  - Materials availability
  - Data and code availability
- METHOD DETAILS
  - Histone proteins
  - Molecular construct for single-molecule experiments
  - Chromatosome reconstitution verification
  - Optical tweezers
  - Data analysis
- QUANTIFICATION AND STATISTICAL ANALYSIS

SUPPLEMENTAL INFORMATION

Supplemental information can be found online at https://doi.org/10.1016/j.molcel.2021.06.006.

ACKNOWLEDGMENTS

We acknowledge support from the Israel Science Foundation (grants 1782/17 to A.K. and 1850/17 to P.M.).

AUTHOR CONTRIBUTIONS

S.R. and Y.G. performed the experiments. S.R. and E.G. prepared experimental materials. S.R. and H.K. analyzed the data. S.R. and A.K. wrote the paper. P.M and A.K. supervised the research.

DECLARATION OF INTERESTS

The authors declare no competing interests.

Received: January 13, 2021
Revised: June 1, 2021
Accepted: June 3, 2021
Published: June 29, 2021

REFERENCES

Allan, J., Hartman, P.G., Crane-Robinson, C., and Aviles, F.X. (1980). The structure of histone H1 and its location in chromatin. Nature *288*, 675–679.

An, W., Leuba, S.H., van Holde, K., and Zlatanova, J. (1998). Linker histone protects linker DNA on only one side of the core particle and in a sequence-dependent manner. Proc. Natl. Acad. Sci. USA *95*, 3396–3401.

Arimura, Y., Shih, R.M., Froom, R., and Funabiki, H. (2020). Nucleosome structural variations in interphase and metaphase chromosomes. bioRxiv. https://doi.org/10.1101/2020.11.12.380386.

Bar-Sadeh, B., Rudnizky, S., Pnueli, L., Bentley, G.R., Stöger, R., Kaplan, A., and Melamed, P. (2020). Unravelling the role of epigenetics in reproductive adaptations to early-life environment. Nat. Rev. Endocrinol. *16*, 519–533.

Bednar, J., Garcia-Saez, I., Boopathi, R., Cutter, A.R., Papai, G., Reymer, A., Syed, S.H., Lone, I.N., Tonchev, O., Crucifix, C., et al. (2017). Structure and Dynamics of a 197 bp Nucleosome in Complex with Linker Histone H1. Mol. Cell *66*, 384–397.e8.

Bernier, M., Luo, Y., Nwokelo, K.C., Goodwin, M., Dreher, S.J., Zhang, P., Parthun, M.R., Fondufe-Mittendorf, Y., Ottesen, J.J., and Poirier, M.G. (2015). Linker histone H1 and H3K56 acetylation are antagonistic regulators of nucleosome dynamics. Nat. Commun. *6*, 10152.

Bockelmann, U., Essevaz-Roulet, B., and Heslot, F. (1998). DNA strand separation studied by single molecule force measurements. Phys. Rev. E Stat. Phys. Plasmas Fluids Relat. Interdiscip. Topics *58*, 2386–2394.

Brown, D.T., Izard, T., and Misteli, T. (2006). Mapping the interaction surface of linker histone H1(0) with the nucleosome of native chromatin in vivo. Nat. Struct. Mol. Biol. *13*, 250–255.

Caterino, T.L., and Hayes, J.J. (2011). Structure of the H1 C-terminal domain and function in chromatin condensation. Biochem. Cell Biol. *89*, 35–44.

Caterino, T.L., Fang, H., and Hayes, J.J. (2011). Nucleosome linker DNA contacts and induces specific folding of the intrinsically disordered H1 carboxyl-terminal domain. Mol. Cell. Biol. *31*, 2341–2348.

Catez, F., Ueda, T., and Bustin, M. (2006). Determinants of histone H1 mobility and chromatin binding in living cells. Nat. Struct. Mol. Biol. *13*, 305–310.

Chen, Z., Gabizon, R., Brown, A.I., Lee, A., Song, A., Díaz-Celis, C., Kaplan, C.D., Koslover, E.F., Yao, T., and Bustamante, C. (2019). High-resolution and high-accuracy topographic and transcriptional maps of the nucleosome barrier. eLife *8*, e48281.

Choppakatla, P., Dekker, B., Cutts, E.E., Vannini, A., Dekker, J., and Funabiki, H. (2020). Linker histone H1.8 inhibits chromatin-binding of condensins and DNA topoisomerase II to tune chromosome compaction and individualization. bioRxiv. https://doi.org/10.1101/2020.12.20.423657.

Christophorou, M.A., Castelo-Branco, G., Halley-Stott, R.P., Oliveira, C.S., Loos, R., Radzisheuskaya, A., Mowen, K.A., Bertone, P., Silva, J.C.R., Zernicka-Goetz, M., et al. (2014). Citrullination regulates pluripotency and histone H1 binding to chromatin. Nature *507*, 104–108.

Chua, E.Y.D., Vasudevan, D., Davey, G.E., Wu, B., and Davey, C.A. (2012). The mechanics behind DNA sequence-dependent properties of the nucleosome. Nucleic Acids Res. *40*, 6338–6352.

Clark, D.J., Hill, C.S., Martin, S.R., and Thomas, J.O. (1988). Alpha-helix in the carboxy-terminal domains of histones H1 and H5. EMBO J. *7*, 69–75.

Claudet, C., Angelov, D., Bouvet, P., Dimitrov, S., and Bednar, J. (2005). Histone octamer instability under single molecule experiment conditions. J. Biol. Chem. *280*, 19958–19965.

Collepardo-Guevara, R., and Schlick, T. (2014). Chromatin fiber polymorphism triggered by variations of DNA linker lengths. Proc. Natl. Acad. Sci. USA *111*, 8061–8066.

Dechassa, M.L., Wyns, K., Li, M., Hall, M.A., Wang, M.D., and Luger, K. (2011). Structure and Scm3-mediated assembly of budding yeast centromeric nucleosomes. Nat. Commun. *2*, 313.

Depken, M., and Schiessel, H. (2009). Nucleosome shape dictates chromatin fiber structure. Biophys. J. *96*, 777–784.

Ericsson, C., Grossbach, U., Björkroth, B., and Daneholt, B. (1990). Presence of histone H1 on an active Balbiani ring gene. Cell *60*, 73–83.

Finch, J.T., and Klug, A. (1976). Solenoidal model for superstructure in chromatin. Proc. Natl. Acad. Sci. USA *73*, 1897–1901.

Fyodorov, D.V., Zhou, B.R., Skoultchi, A.I., and Bai, Y. (2018). Emerging roles of linker histones in regulating chromatin structure and function. Nat. Rev. Mol. Cell Biol. *19*, 192–206.

Garcia-Saez, I., Menoni, H., Boopathi, R., Shukla, M.S., Soueidan, L., Noirclerc-Savoye, M., Le Roy, A., Skoufias, D.A., Bednar, J., Hamiche, A., et al. (2018). Structure of an H1-Bound 6-Nucleosome Array Reveals an Untwisted Two-Start Chromatin Fiber Conformation. Mol. Cell *72*, 902–915.e7.

Gibbs, E.B., and Kriwacki, R.W. (2018). Linker histones as liquid-like glue for chromatin. Proc. Natl. Acad. Sci. USA *115*, 11868–11870.

Gibson, B.A., Doolittle, L.K., Schneider, M.W.G., Jensen, L.E., Gamarra, N., Henry, L., Gerlich, D.W., Redding, S., and Rosen, M.K. (2019). Organization of Chromatin by Intrinsic and Regulated Phase Separation. Cell *179*, 470–484.e21.

Gilbert, N. (2019). Biophysical regulation of local chromatin structure. Curr. Opin. Genet. Dev. *55*, 66–75.

Gittes, F., and Schmidt, C.F. (1998). Interference model for back-focal-plane displacement detection in optical tweezers. Opt. Lett. *23*, 7–9.

Goddard, T.D., Huang, C.C., Meng, E.C., Pettersen, E.F., Couch, G.S., Morris, J.H., and Ferrin, T.E. (2018). UCSF ChimeraX: Meeting modern challenges in visualization and analysis. Protein Science *27*.

Hall, M.A., Shundrovsky, A., Bai, L., Fulbright, R.M., Lis, J.T., and Wang, M.D. (2009). High-resolution dynamic mapping of histone-DNA interactions in a nucleosome. Nat. Struct. Mol. Biol. *16*, 124–129.

Hamiche, A., Schultz, P., Ramakrishnan, V., Oudet, P., and Prunell, A. (1996). Linker histone-dependent DNA structure in linear mononucleosomes. J. Mol. Biol. *257*, 30–42.

Hao, F., Murphy, K.J., Kujirai, T., Kamo, N., Kato, J., Koyama, M., Okamato, A., Hayashi, G., Kurumizaka, H., and Hayes, J.J. (2020). Acetylation-modulated communication between the H3 N-terminal tail domain and the intrinsically disordered H1 C-terminal domain. Nucleic Acids Res. *48*, 11510–11520.

Hayashihara, K., Zlatanova, J., and Tomschik, M. (2010). Simplified method for recombinant linker histone H1 purification. Mol. Biotechnol. *44*, 148–151.

Hayes, J.J., Pruss, D., and Wolffe, A.P. (1994). Contacts of the globular domain of histone H5 and core histones with DNA in a "chromatosome". Proc. Natl. Acad. Sci. USA *91*, 7817–7821.

Heidarsson, P.O., Mercadante, D., Sottini, A., Nettels, D., Borgia, M.B., Borgia, A., Kilic, S., Fierz, B., Best, R.B., and Schuler, B. (2020). Disordered Proteins Enable Histone Chaperoning on the Nucleosome. bioRxiv, 2020.04.17.046243.

Hendzel, M.J., Lever, M.A., Crawford, E., and Th'ng, J.P.H. (2004). The C-terminal domain is the primary determinant of histone H1 binding to chromatin in vivo. J. Biol. Chem. *279*, 20028–20034.

Hodges, C., Bintu, L., Lubkowska, L., Kashlev, M., and Bustamante, C. (2009). Nucleosomal fluctuations govern the transcription dynamics of RNA polymerase II. Science *325*, 626–628.

Koch, S.J., Shundrovsky, A., Jantzen, B.C., and Wang, M.D. (2002). Probing protein-DNA interactions by unzipping a single DNA double helix. Biophys. J. *83*, 1098–1105.

Kornberg, R.D. (1974). Chromatin structure: a repeating unit of histones and DNA. Science *184*, 868–871.

Kornberg, R.D., and Thomas, J.O. (1974). Chromatin structure; oligomers of the histones. Science *184*, 865–868.

Li, W., Chen, P., Yu, J., Dong, L., Liang, D., Feng, J., Yan, J., Wang, P.Y., Li, Q., Zhang, Z., et al. (2016). FACT Remodels the Tetranucleosomal Unit of Chromatin Fibers for Gene Transcription. Mol. Cell *64*, 120–133.

Lowary, P.T., and Widom, J. (1998). New DNA sequence rules for high affinity binding to histone octamer and sequence-directed nucleosome positioning. J. Mol. Biol. *276*, 19–42.

Luger, K., Mäder, A.W., Richmond, R.K., Sargent, D.F., and Richmond, T.J. (1997). Crystal structure of the nucleosome core particle at 2.8 A resolution. Nature *389*, 251–260.

Malik, O., Khamis, H., Rudnizky, S., Marx, A., and Kaplan, A. (2017). Pausing kinetics dominates strand-displacement polymerization by reverse transcriptase. Nucleic Acids Res. *45*, 10190–10205.

McGhee, J.D., and Felsenfeld, G. (1980). Nucleosome structure. Annu. Rev. Biochem. *49*, 1115–1156.

Nacheva, G.A., Guschin, D.Y., Preobrazhenskaya, O.V., Karpov, V.L., Ebralidse, K.K., and Mirzabekov, A.D. (1989). Change in the pattern of histone binding to DNA upon transcriptional activation. Cell *58*, 27–36.

Noll, M., and Kornberg, R.D. (1977). Action of micrococcal nuclease on chromatin and the location of histone H1. J. Mol. Biol. *109*, 393–404.

Olins, A.L., and Olins, D.E. (1974). Spheroid chromatin units (v bodies). Science *183*, 330–332.

Olins, D.E., and Olins, A.L. (2003). Chromatin history: our view from the bridge. Nat. Rev. Mol. Cell Biol. *4*, 809–814.

Ou, H.D., Phan, S., Deerinck, T.J., Thor, A., Ellisman, M.H., and O'Shea, C.C. (2017). ChromEMT: Visualizing 3D chromatin structure and compaction in interphase and mitotic cells. Science *357*, eaag0025.

Öztürk, M.A., Cojocaru, V., and Wade, R.C. (2018a). Toward an Ensemble View of Chromatosome Structure: A Paradigm Shift from One to Many. Structure *26*, 1050–1057.

Öztürk, M.A., Cojocaru, V., and Wade, R.C. (2018b). Dependence of Chromatosome Structure on Linker Histone Sequence and Posttranslational Modification. Biophys. J. *114*, 2363–2375.

Öztürk, M.A., De, M., Cojocaru, V., and Wade, R.C. (2020). Chromatosome Structure and Dynamics from Molecular Simulations. Annu. Rev. Phys. Chem. *71*, 101–119.

Perišić, O., Portillo-Ledesma, S., and Schlick, T. (2019). Sensitive effect of linker histone binding mode and subtype on chromatin condensation. Nucleic Acids Res. *47*, 4948–4957.

Prendergast, L., and Reinberg, D. (2021). The missing link*er*: emerging trends for H1 variant-specific functions. Genes Dev. *35*, 40–58.

Pruss, D., Bartholomew, B., Persinger, J., Hayes, J., Arents, G., Moudrianakis, E.N., and Wolffe, A.P. (1996). An asymmetric model for the nucleosome: a binding site for linker histones inside the DNA gyres. Science *274*, 614–617.

Ricci, M.A., Manzo, C., García-Parajo, M.F., Lakadamyali, M., and Cosma, M.P. (2015). Chromatin fibers are formed by heterogeneous groups of nucleosomes in vivo. Cell *160*, 1145–1158.

Roque, A., Ponte, I., and Suau, P. (2009). Role of charge neutralization in the folding of the carboxy-terminal domain of histone H1. J. Phys. Chem. B *113*, 12061–12066.

Rudnizky, S., Bavly, A., Malik, O., Pnueli, L., Melamed, P., and Kaplan, A. (2016). H2A.Z controls the stability and mobility of nucleosomes to regulate expression of the LH genes. Nat. Commun. *7*, 12958.

Rudnizky, S., Khamis, H., Malik, O., Squires, A.H., Meller, A., Melamed, P., and Kaplan, A. (2018). Single-molecule DNA unzipping reveals asymmetric modulation of a transcription factor by its binding site sequence and context. Nucleic Acids Res. *46*, 1513–1524.

Rudnizky, S., Khamis, H., Malik, O., Melamed, P., and Kaplan, A. (2019). The base pair-scale diffusion of nucleosomes modulates binding of transcription factors. Proc. Natl. Acad. Sci. USA *116*, 12161–12166.

Simpson, R.T. (1978). Structure of the chromatosome, a chromatin particle containing 160 base pairs of DNA and all the histones. Biochemistry *17*, 5524–5531.

Song, F., Chen, P., Sun, D., Wang, M., Dong, L., Liang, D., Xu, R.M., Zhu, P., and Li, G. (2014). Cryo-EM study of the chromatin fiber reveals a double helix twisted by tetranucleosomal units. Science *344*, 376–380.

Syed, S.H., Goutte-Gattat, D., Becker, N., Meyer, S., Shukla, M.S., Hayes, J.J., Everaers, R., Angelov, D., Bednar, J., and Dimitrov, S. (2010). Single-base resolution mapping of H1-nucleosome interactions and 3D organization of the nucleosome. Proc. Natl. Acad. Sci. USA *107*, 9620–9625.

Tolić-Nørrelykke, S.F., Schäffer, E., Howard, J., Pavone, F.S., Jülicher, F., and Flyvbjerg, H. (2006). Calibration of optical tweezers with positional detection in the back focal plane. Rev. Sci. Instrum. *77*, 103101.

Torres, C.M., Biran, A., Burney, M.J., Patel, H., Henser-Brownhill, T., Cohen, A.S., Li, Y., Ben-Hamo, R., Nye, E., Spencer-Dene, B., et al. (2016). The linker histone H1.0 generates epigenetic and functional intratumor heterogeneity. Science *353*, aaf1644.

Turner, A.L., Watson, M., Wilkins, O.G., Cato, L., Travers, A., Thomas, J.O., and Stott, K. (2018). Highly disordered histone H1-DNA model complexes and their condensates. Proc. Natl. Acad. Sci. USA *115*, 11964–11969.

White, A.E., Hieb, A.R., and Luger, K. (2016). A quantitative investigation of linker histone interactions with nucleosomes and chromatin. Sci. Rep. *6*, 19122.

Widom, J. (1998). Chromatin structure: linking structure to function with histone H1. Curr. Biol. *8*, R788–R791.

Willcockson, M.A., Healton, S.E., Weiss, C.N., Bartholdy, B.A., Botbol, Y., Mishra, L.N., Sidhwani, D.S., Wilson, T.J., Pinto, H.B., Maron, M.I., et al. (2021). H1 histones control the epigenetic landscape by local chromatin compaction. Nature *589*, 293–298.

Wiśniewski, J.R., Zougman, A., Krüger, S., and Mann, M. (2007). Mass spectrometric mapping of linker histone H1 variants reveals multiple acetylations, methylations, and phosphorylation as well as differences between cell culture and tissue. Mol. Cell. Proteomics *6*, 72–87.

Wiśniewski, J.R., Zougman, A., and Mann, M. (2008). Nepsilon-formylation of lysine is a widespread post-translational modification of nuclear proteins occurring at residues involved in regulation of chromatin function. Nucleic Acids Res. *36*, 570–577.

Woodcock, C.L., and Dimitrov, S. (2001). Higher-order structure of chromatin and chromosomes. Curr. Opin. Genet. Dev. *11*, 130–135.

Woods, D.C., and Wereszczynski, J. (2020). Elucidating the influence of linker histone variants on chromatosome dynamics and energetics. Nucleic Acids Res. *48*, 3591–3604.

Yusufova, N., Kloetgen, A., Teater, M., Osunsade, A., Camarillo, J.M., Chin, C.R., Doane, A.S., Venters, B.J., Portillo-Ledesma, S., Conway, J., et al. (2021). Histone H1 loss drives lymphoma by disrupting 3D chromatin architecture. Nature *589*, 299–305.

Zhang, Y., Smith, C.L., Saha, A., Grill, S.W., Mihardja, S., Smith, S.B., Cairns, B.R., Peterson, C.L., and Bustamante, C. (2006). DNA translocation and loop formation mechanism of chromatin remodeling by SWI/SNF and RSC. Mol. Cell *24*, 559–568.

Zhou, B.R., Feng, H., Kato, H., Dai, L., Yang, Y., Zhou, Y., and Bai, Y. (2013). Structural insights into the histone H1-nucleosome complex. Proc. Natl. Acad. Sci. USA *110*, 19390–19395.

Zhou, B.R., Jiang, J., Feng, H., Ghirlando, R., Xiao, T.S., and Bai, Y. (2015). Structural Mechanisms of Nucleosome Recognition by Linker Histones. Mol. Cell *59*, 628–638.

Zhou, B.R., Feng, H., Ghirlando, R., Li, S., Schwieters, C.D., and Bai, Y. (2016). A Small Number of Residues Can Determine if Linker Histones Are Bound On or Off Dyad in the Chromatosome. J. Mol. Biol. *428*, 3948–3959.

Zhou, B.R., Feng, H., Kale, S., Fox, T., Khant, H., de Val, N., Ghirlando, R., Panchenko, A.R., and Bai, Y. (2021). Distinct Structures and Dynamics of Chromatosomes with Different Human Linker Histone Isoforms. Mol. Cell *81*, 166–182.e6.

STAR★METHODS

KEY RESOURCES TABLE

REAGENT or RESOURCE	SOURCE	IDENTIFIER
Antibodies		
Polyclonal sheep Anti-digoxigenin	Roche	Cat#11333089001; RRID:AB_514496
Bacterial and virus strains		
Escherichia coli BL21-CodonPlus (DE3)-RIPL Competent Cells	Agilent	Cat#230280
Escherichia coli Rosetta(DE3) pLysS Competent Cells	Novagen	Cat#70956
Chemicals, peptides, and recombinant proteins		
Hydroxylapatite, Fast Flow column	Millipore	Cat#391947
Sulfopropyl Sepharose	Sigma-Aldrich	Cat#S1799
Casein hydrolysate	Sigma-Aldrich	Cat#22090
Bovin Serum Albumin (BSA)	Sigma-Aldrich	Cat#A2153
cOmplete EDTA-free protease inhibitor cocktail	Roche	Cat#5056489001
Red load taq master	Larova	Cat#PCR-108
Q5 High-fidelity DNA polymerase	New England Biolabs	Cat#M0491L
Rapid Ligation Buffer	Promega	Cat#C6711
T4 DNA ligase	New England Biolabs	Cat#M0202S/M
T4 Polynucleotide Kinase	New England Biolabs	Cat#M0201L
DraIII-HF	New England Biolabs	Cat#R3510L
BglI	New England Biolabs	Cat#R0143L
Human H2A/H2B	New England Biolabs	Cat#M2508S
Human H3.1/H4	New England Biolabs	Cat#M2509S
Human H1.0	New England Biolabs	Cat#M2501S
Mouse H1.0K69A	This study	N/A
Mouse H1.0Δ(97)CTD	This study	N/A
Mouse H1.0Δ72	This study	N/A
Mouse H1.0Δ48	This study	N/A
Mouse H1.0Δ24	This study	N/A
Mouse H1.0K153E	This study	N/A
Crtitical Commercial Assays		
QIAquick PCR Purification Kit	QIAGEN	Cat#28106
QIAquick Gel Extraction Kit	QIAGEN	Cat#28706
Oligonucleotides		
Primers for site-directed mutagenesis (see Table S1)	This study	N/A
Primers for making DNA templates (see Tables S1 and S2)	This study	N/A
Recombinant DNA		
DNA constructs for unzipping (Table S3)	This study	N/A
DNA handles	Rudnizky et al., 2019	N/A
pColaduet-1 expression vector	Merck	Cat#71406
pGEM-T easy	Promega	Cat#A137A
aT3-cells genomic DNA	Rudnizky et al., 2016	N/A
601 DNA	Rudnizky et al., 2016	N/A
Lambda DNA	New England Biolabs	Cat#N3011S

(*Continued on next page*)

Continued

REAGENT or RESOURCE	SOURCE	IDENTIFIER
Software and algorithms		
Chimerax	Goddard et al., 2018	https://www.cgl.ucsf.edu/chimerax/
LabVIEW VIs for instrument control, data acquisition, and data analysis	Rudnizky et al., 2016	N/A
MATLAB scripts for data analysis	This study	N/A
Snapgene viewer	Snapgene	https://www.snapgene.com/
Other		
Dual optical trap setup	Rudnizky et al., 2016	N/A
Multi-channel laminar flow cell	Lumicks	u-Flux
Slide-A-Lyzer MINI dialysis units 7000 MWCO	Thermo-scientific	Cat#69562
Amicon Ultra	Merck	Cat#UFC900324
Gradient SDS-PAGE	BioRad	Cat#456-1094
0.84 μm Protein-G polystyrene bead	Spherotech	Cat#PGP-8-5
0.9 μm streptavidin polystyrene bead	Spherotech	Cat#SVP-08-10

RESOURCE AVAILABILITY

Lead contact

Further information and requests for resources and reagents should be directed to and will be fulfilled by the lead contact, Ariel Kaplan (akaplanz@technion.ac.il).

Materials availability

All unique/stable reagents generated in this study are available from the Lead Contact with a completed Materials Transfer Agreement.

Data and code availability

The published article includes all relevant data generated or analyzed during this study. Additional data and codes are available from the corresponding author on request.

METHOD DETAILS

Histone proteins

The mH1.0 ORF was amplified from mouse cDNA using PCR with primers listed in Table S1. The product was cloned into a pColaduet-1 expression vector (71406; Merck). The H1K69A, H1T153E, and H1ΔCTD mutations were generated from WT mH1.0 in pColaduet-1 using primers listed in Table S1. All constructs were verified by sequencing. The proteins were expressed in *E. coli* Rosetta or CodonPlus-RIPL (DE3), grown for 5 h at 37 °C in LB and induced with 1 mM isopropyl-β-D-thiogalactoside at 18 °C overnight. The proteins were purified as described previously (Hayashihara et al., 2010) with the following modifications: The sonicated pellets were loaded into a Hydroxylapatite, Fast Flow column (391947; Millipore) pre-equilibrated with 25 mM phosphate buffer, pH 6.8, and eluted with 25 mM phosphate buffer + 1.5 M NaCl, pH 6.8. Late fractions were pooled and diluted in a 25 mM phosphate buffer to a final concentration of 50 mM NaCl. The eluates were loaded on a Sulfopropyl (SP) Sepharose column (S1799; Sigma), washed with ten volumes of 25 mM phosphate buffer + 0.5 M NaCl, pH 6.8 and eluted with 25 mM phosphate buffer + 1.5 M NaCl, pH 6.8 for WT H1, H1K69A, and H1T153E variants. The fractions containing H1ΔCTD(97), H1Δ72, H1Δ48 and H1Δ24 mutants were loaded on a SP column, washed with 50 mM Tris-Cl, 2mM EDTA, 0.3 M NaCl, pH 8 and eluted using 50 mM Tris-Cl, 2mM EDTA, 0.6 M NaCl, pH 8. All fractions were concentrated using Amicon Ultra (UFC900324; Merck), snap-frozen and kept at −80°C. All buffers were supplemented with a cOmplete EDTA-free protease inhibitor cocktail (5056489001; Roche). Protein sequences of H1 proteins are summarized in Table S5.

Histones H1 (M2501S; NEB), H2A/H2B (M2508S; NEB), and H3.1/H4 (M2509S; NEB) from human origin were all purchased from NEB. The H2A/H2B and H3.1/H4 were mixed in $2(H2A/H2B)_2$:$1(H3/H4)_4$ molar ratio to form octamers.

Molecular construct for single-molecule experiments

For PCR-based nucleosomal DNA segments, a ~234 bp fragment of DNA containing the Widom 601 positioning sequence and a ~249 bp fragment corresponding to the −1/+223 region of the mouse *Cga* gene (Rudnizky et al., 2016) were amplified using standard PCR reactions with primers listed in Table S1. The constructs were digested with DraIII-HF(R3510L; NEB) or BglI (R0143L; NEB)

overnight according to the manufacturer's instructions, purified using a QIAquick PCR Purification Kit (28106; QIAGEN) and mixed with recombinant histone octamers to form mono-nucleosomes under conditions reported (Rudnizky et al., 2016). For ligation-based nucleosomal DNA segments (e.g., 601-AT), oligos listed in Table S2 were purchased from IDT and phosphorylated using T4 Polynucleotide Kinase (M0201L; NEB) according to the manufacturer's instructions. For each type of construct, oligos were mixed in a 1:1 molar ratio with their complementary sequence, as shown in Table S2. Each mix was incubated at 90°C for 5 min and annealed in 1x T4 DNA Ligase Reaction Buffer (B0202S; NEB) by gradual cooling. Each annealing reaction led to the formation of dsDNA fragment, flanked by unique sticky overhangs designed to ligate the next dsDNA fragment in a chain. The fragments were ligated using concentrated T4 DNA ligase (M0202M; NEB) and purified using a QIAquick Gel Extraction Kit (28706; QIAGEN) to form constructs listed in Table S3, which were used for nucleosome reconstitution. DNA sequences used in each experiment are summarized in Table S6.

Two ~2000-bp DNA handles were generated as previously reported (Rudnizky et al., 2019), ligated to the alignment segment amplified with primers listed in Table S1 and digested with DraIII-HF. The construct was kept at −20°C prior to usage.

Reconstituted nucleosomes were ligated to the DNA handles using T4 DNA ligase (M0202S; NEB) and 1x Rapid Ligation Buffer (C6711; Promega) in a 3:1 molar ratio, 16 h at 4°C overnight. The full construct (i.e., handles + alignment segment + nucleosome) was incubated for 15 min on ice with 0.8 μm polystyrene beads (Spherotech) coated with anti-digoxygenin. The reaction was then diluted 500-fold in H1 buffer (10 mM Tris·Cl (pH 8), 1 mM EDTA, 50 mM NaCl, 1 mM DTT, 5% v/v glycerol and 150 ng/μl BSA). Tether formation was performed inside the experimental chamber by trapping an anti-dig bead (bound by nucleosomes) in one trap, trapping a 0.9 μm streptavidin-coated polystyrene bead in the second trap, and bringing the two beads into proximity to allow binding of the biotin tag in the nucleosomal DNA to the streptavidin on the bead. The trapped nucleosome was incubated ~30 s with 5 nM of H1 in H1 buffer to form chromatosomes, after which the complex was moved to the H1-free region and unzipped (see Figure 1A).

Chromatosome reconstitution verification

The correct H1:nucleosome stoichiometry (1:1) was confirmed by the following control experiments: (1) Gel shift experiments showed a single population of chromatosomes at the concentration used in single-molecule experiments. In addition, in these conditions, ~50% of nucleosomes were H1 free, indicating subsaturating conditions. (2) The alignment sequence, which was used to monitor non-specific binding or accumulation of H1 on naked DNA, showed an identical unzipping pattern in the presence or absence of H1 (Figures 1C and S1H). (3) The binding of H1 to bare DNA was not observed in the absence of nucleosome (Figures S1J–S1M) (4). The magnitude of H3-NTD rupture forces, which serve as a proxy for H1 binding, remained identical when H1 concentration was reduced fivefold (Figure S1I).

In addition, the structural integrity of H1-nucleosome complex is supported by the following observations: (1) A similar stabilization of major histone-DNA interactions was observed using the bacterially expressed mouse H1 (mH1), as with commercially available human H1 (hH1) (M2501S; NEB), sharing 96.5% identity with mH1 (Figures S1H and S1I). (2) Despite their rapid dissociation, we were able to unzip a small number of chromatosomes formed in bulk and transferred to the optical tweezers; an identical stabilization of H3-NTD was detected for these chromatosomes and the chromatosomes formed *in situ* under single-molecule conditions (Figure S1I) (3) The pattern of stabilization was similar for all H1 proteins and DNA sequences tested (i.e., 601, *Cga*, 601-AT).

Optical tweezers

Experiments were performed in a custom-made dual-trap optical tweezers apparatus, as previously reported (Malik et al., 2017; Rudnizky et al., 2016, 2019). Briefly, the beam from a 855 nm laser (TA PRO, Toptica) was coupled into a polarization-maintaining single-mode optical fiber. The collimated beam out of the fiber was split by a polarizing beam splitter (PBS) into two orthogonal polarizations, each directed into a mirror and combined again with a second BS. One of the mirrors is mounted on a nanometer scale mirror mount (Nano-MTA, Mad City Labs). A X2 telescope expands the beam, and also images the plane of the mirrors into the back focal plane of the focusing microscope objective (Nikon, Plan Apo VC 60X, NA/1.2). Two optical traps are formed at the objective's focal plane, each by a different polarization, and with a typical stiffness of 0.3-0.5 pN/nm. The light is collected by a second, identical objective, the two polarizations separated by a PBS, and imaged onto two Position Sensitive Detectors (First Sensor). The position of the beads relative to the center of the trap is determined by back focal plane interferometry (Gittes and Schmidt, 1998). Calibration of the setup was done by analysis of the thermal fluctuations of the trapped beads (Tolić-Nørrelykke et al., 2006), which were sampled at 100kHz. Experiments were conducted using a laminar flow cell (u-Flux, Lumicks).

Data analysis

Calibration of the setup was done by analysis of the thermal fluctuations of the trapped beads, which were sampled at 100 kHz. Experimental data were digitized at a 2500 Hz and converted into force and extension vectors using the calibration parameters. To precisely determine and subtract any residual offset in the extension of individual experiments, force-extension curves were fitted, up to 15 pN, to an extensible worm-like-chain (eWLC) model of double-stranded DNA with persistence length 45 nm, contour length per base pair 0.34 nm/bp and stretch modulus 1000 pN. Then, to calculate the number of unzipped base pairs we divided the extension by twice the contour length of a ssDNA nucleotide, calculated with a WLC model with persistence length 1 nm and contour length per nucleotide 0.64 nm/nt. The 248 bp naked DNA alignment segment was used to perform a correlation-based alignment of all

traces in an experiment. The 'distance from dyad' in force-position curves was calculated by subtracting the known position of the nucleosome's center at each construct: 360 bp for a 601 DNA, and 486 bp for 601-AT.

In full, irreversible unzipping experiments (Figures 1, 2, S1A–C, S1E, S1H, and S4) the steerable trap was continuously moved at 280 nm/s to stretch the tethered construct, until the nucleosome fully disassembled. In the repetitive/reversible unzipping experiments (Figures 3, 4, 5, S1I, S2, S3, and S6), the steerable trap was moved only until the fork reaches the point where the nucleosome's proximal H2A/H2B is identified (typically ~19-22 pN). At this point, the steering direction is reversed, thus relaxing the force and allowing the DNA to reanneal. Each tethered complex was first reversibly unzipped 10 times in the absence of H1 (control experiment) and then reversibly unzipped 10-80 times in the presence of H1 (experimental traces), with a cycle time of 8 s, unless specified. Data were low-pass filtered for further analysis with a zero phase Butterworth filter, with a bandwidth of 40 and 150 Hz for the irreversible and reversible unzipping experiments, respectively.

Force-weighted (FW) dwell time histograms (Figures 1F, 1G, 2B, and 2C) were calculated similarly to previously reported (Chen et al., 2019; Hall et al., 2009). We counted the number of data points in 1 bp bins, and divided by the sampling rate (2500 Hz) multiplied by the detected rupture force, after subtracting the average background signal of naked DNA. Averaged force-position traces (Figures 2D, 2E, S4B, S1M, and S2E–S2G) were calculated by resampling (i.e., interpolating) the force vectors of different traces into a common uniformly-spaced 1 bp array, and averaging the interpolated forces.

To calculate the mean breaking force in a specific region, we generated an ''interaction vector'' for each trace, where an interaction is defined as an increase in force at constant position, followed by a force drop (a break). FW dwell time histograms were used to detect clusters of interactions corresponding to specific histone-DNA interactions (i.e., H3-NTD, H2A/H2B, H3/H4 for Figures 1 and 2) and determine their boundaries. The interaction with the highest breaking force inside the boundaries of each region defines the region's breaking force, which is then averaged over the ensemble.

Given the clear separation of rupture forces in experiments with or without H1 in all clusters of interactions (Figures S5A and S5B), we identified ''bound'' events as interactions with higher breaking force than that of the same region in the control experiments, plus twice its standard deviation. Applying the same criteria for the data obtained without H1 resulted in detection of less than 1.5% of the events detected with H1. The binding probability is defined as the number of bound events detected at a specific cycle out of the total number of experiments and is shown only for data containing at least 5 experiments. Notably, for all the interaction regions, these probabilities are independent of the ''incubation time,'' i.e., the time before the interaction is probed (Figure S3A), indicating that the system is in thermodynamic equilibrium and the measured probability reflects the energy of the interaction (Koch et al., 2002; Rudnizky et al., 2018). Mean forces were calculated by averaging the breaking force of all the detected bound events in a certain region. Only data calculated from more than 2 data points (i.e., 2 bound events) are shown in Figures 3C and S2D. For the longer invasion experiments, the data were calculated over ten-cycle windows in order to increase the data points at each window. The mean breaking force is presented only if more than two data points were identified as being bound at each window, and the probability is presented only if at least 10 experiments exist.

QUANTIFICATION AND STATISTICAL ANALYSIS

Statistical details for the individual experiments, including the number of observations, the type and magnitude of the calculated uncertainties, and the identity and results of statistical tests, when relevant, are described in the figure legends and in Table S4.